

The design and fabrication of autonomous polymer-based surface tension-confined microfluidic platforms

Michael J. Swickrath · Suresh Shenoy ·
J. Adin Mann Jr. · Jim Belcher ·
Robert Kovar · Gary E. Wnek

Received: 27 July 2007 / Accepted: 26 September 2007 / Published online: 13 October 2007
© Springer-Verlag 2007

Abstract A one-step thick film printing process has been established for patterning hydrophobic polyvinyl chloride (PVC) substrate materials with hydrophilic cellulose acetate. The opposing patterned substrate materials are brought within close proximity utilizing spacer material of defined thickness. The parallel-plate configured devices are capable of supporting autonomous fluid transport through capillarity. Minimum attainable path widths of $313.3 \pm 17.9 \mu\text{m}$ can be achieved utilizing an affordable personal printer for photomask generation. In addition, a theoretical model for this system predicting meniscus position as a function of time and system architecture is posed along with experimental data which is found to be in good agreement with the model. Lastly, the curvature of the surface is approximated and exploited for the determination of the true pressure jump across the curved surface at the gas–liquid interface at all points on a discretized surface. The curvature associated pressure jump results are found to be consistent with the Laplace pressure approximation.

Keywords Surface-directed microfluidics · Surface tension-confined · Capillary microfluidics · Monge representation · Thick film printing

1 Introduction

Microfluidic and “lab on a chip” technology is speculated to revolutionize the way in which chemical and biological analyses are conducted. Such devices promise the capacity to manipulate micro-volumes of fluid in order to maximize throughput with greater degrees of parallelization while minimizing the amount expensive and/or invasive reagent. To date, several novel microfluidic systems have been developed demonstrating the automation of clinical techniques such as the enzyme-linked immunosorbent assay (Eteshola and Balberg 2004; Eteshola and Leckband 2001; Sato et al. 2004) and DNA analyses (Burns 1998; Khandurina et al. 2000; Lagally et al. 2000; Mastrangelo et al. 1998), as well as novel applications for fuel cell development and optimization (Choban et al. 2004; Jayashree et al. 2005; Mitrovski et al. 2004).

However, the anticipated impact of microfluidic technology has yet to have materialized for a combination of reasons. For example, fabrication methods can be cost ineffective and time intensive. Furthermore, most platform manufacturing techniques require batch processing rather than continuous production. In addition, platform implementation may require auxiliary hardware such as thermal elements, pumping systems and equipment for optical detection further complicating the platform design rendering the device susceptible to component failure and overall device malfunction. Consequently, before microfluidic technology can be deployed on a wide-scale, it is essential to develop manufacturing methodology with

M. J. Swickrath (✉) · S. Shenoy · J. A. Mann Jr.
Department of Chemical Engineering,
Case Western Reserve University, 10900 Euclid Ave.,
Cleveland, OH 44106, USA
e-mail: mjs60@case.edu

J. Belcher · R. Kovar
Materials Science Division, Infoscitex Corporation,
303 Bear Hill Rd., Waltham, MA 02451, USA

G. E. Wnek
Department of Macromolecular Science and Engineering,
Case Western Reserve University,
10900 Euclid Ave., Cleveland, OH 44106, USA

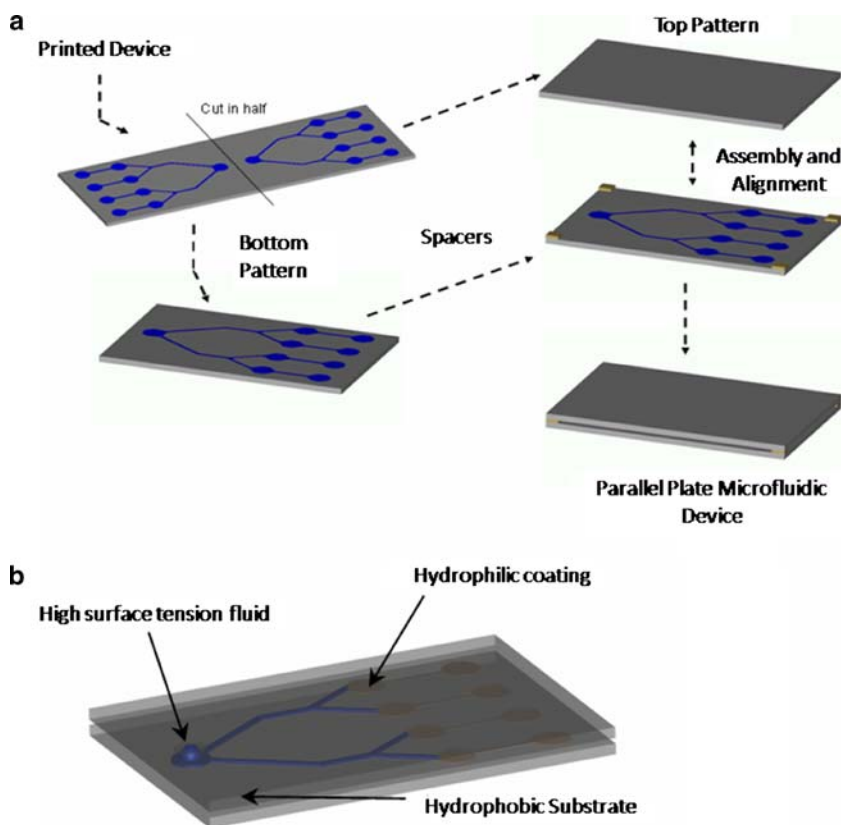
limited rigor as well as designing micro-devices capable of autonomous fluid manipulation.

An alternative paradigm to microfluidic processing involves patterning abrupt discontinuities in surface energy upon a substrate. Consequently, high surface tension fluids can be confined upon regions of higher surface energy in spite of the lack of physical barriers. Patterned substrates are aligned and fixed to each other with intermediate spacers (Fig. 1). Following the introduction of a high surface tension fluid, spontaneous capillary wicking occurs as a result of a pressure drop associated with a curved surface. Moreover, confinement is achieved at the three-phase hydrophobic interface via fluid–substrate energetics. This technique was first employed for capillary electrophoresis (Oh 1999). Subsequently, other groups have further investigated methods to fabricate similar devices via sol gel processing (Lam et al. 2002), monolayer development with octadecyltrichlorosilane by multi-stream laminar flow or photolithography (Bouaidat et al. 2005; Suk and Cho 2007; Zhao et al. 2001, 2002) and even simple methods such as painting hydrophobic barriers (Nag et al. 2005). Recently, a technique has been employed using a microplasma jet to create hydrophilic pathways on chemically-modified hydrophobic glass resulting in parallel-plate millifluidic systems (West et al. 2007). These techniques demonstrate the efficacy of employing two-

dimensional surface energy discontinuities to support autonomous microfluidic transport.

Recently, efforts have been made to exploit microfabrication technology in order to develop manufacturing methodology conducive to mass production. For example, Watanabe has produced autonomous microfluidic platforms via inkjet printing of highly water soluble paths upon a hydrophobic substrate material capable of directing surface flow (Watanabe 2007). Described herein is an alternative fabrication method involving the thick film printing of cellulose acetate upon a polyvinyl chloride (PVC) substrate material. The one-step patterning of these materials develops adequate disparity in surface energy to facilitate spontaneous fluid transport and excellent confinement of aqueous solutions upon the hydrophilic cellulose acetate paths. Furthermore, cellulose acetate is an attractive material as it has already demonstrated compatibility with biological components (Goodwin et al. 1995; Marengo-Rowe 1965; Meera Khan 1971) as opposed to other common materials utilized in the development of microfluidic platforms such as polydimethylsiloxane (Butler et al. 1997a, b). Lastly, thick film printing is an established process thoroughly understood and documented having been around for nearly 40 years (Holmes 1976; White and Turner 1997). Consequently, optimization is

Fig. 1 **a** Configuration of surface-directed microfluidic platform from printed substrate to parallel-plate microfluidic device. **b** Implementation of surface tension confined microfluidic device



straightforward minimizing the rigor associated with implementing mass-production processing. Moreover the choice of commodity polymeric materials such as PVC and cellulose acetate assist in mitigating the device manufacturing cost. Furthermore, the mechanical properties of the PVC substrate material are more advantageous for on-site application than brittle materials such as silicon or glass. Ultimately, the authors envision the one-step production scheme amenable to mass-production implemented continuously.

2 Materials and methods

2.1 Determination of device geometry

The consideration of system energetics lends insight into geometrical criteria required for spontaneous capillary flow. Figure 2, produced via minimizing a free energy through a gradient descent method via the Surface Evolver software package (Brakke 1992), depicts the expected geometry of a fluid filament undergoing capillary transport in a surface-directed platform. Specifically, for the geometry and orientation demonstrated in Fig. 2, the free energy, G , associated with a fluid of surface tension γ wetting a substrate for a length l dependent upon a gap height h and path width w of a material characterized by an advancing contact angle θ as follows (Adamson and Gast 1997; Lam et al. 2002):

$$\frac{dG}{dl} = \gamma(h - w \cos \theta) \tag{1}$$

Consequently, in order to satisfy a negative free energy required for the surface-directed device to support spontaneous flow, the gap height must be less than the product of hydrophilic path width and the cosine of the advancing contact angle

$$h < w \cos \theta. \tag{2}$$

In addition, it is apparent that materials with contact angle greater than or equal to 90° are incapable of supporting capillary transport. One can also arrive at the same result

based on arguments of achieving a negative pressure drop (Zhao et al. 2001, 2002).

For model verification, devices were configured with gap heights of 116.4 ± 7.6 and $229.0 \pm 13.9 \mu\text{m}$ along with varying nominal path widths between 830.9 ± 35.5 and $1352.1 \pm 16.0 \mu\text{m}$. Although these dimensions are rather high with regard to microfluidic device design, the larger widths aid in substrate assembly mitigating experimental error associated with misalignment. However, a wide variety of patterns are demonstrated (Fig. 4) that employ minimal amounts of fluid for device implementation.

2.2 Screen development

Thick film printing screens were made through a one-time photolithographic technique. Patterns are developed with computer-aided drafting software and transferred to transparency films through a Dell Laser Printer 1700 for the development of a photomask. The photomask is utilized on emulsion film (Five Star, Autotype) via exposure to UV in dark room conditions for 3 min and 45 s. The emulsion film is subsequently developed in 1.5% (v/v) hydrogen peroxide solution for one minute. After development, the film is sprayed with copious amounts of warm tap water ($\sim 50^\circ\text{C}$). At this point, the pattern should be evident in the film. The developed film is now placed in cool distilled water for thirty seconds ($\sim 20^\circ\text{C}$). The film is transferred to a 325 mesh stainless steel screen with 0.0011 in. wire diameter via applying pressure with a roller. After subsequent drying time (~ 1 h at 35°C), the plastic coating is peeled from the emulsion film resulting in a patterned screen. The entire process takes approximately 1.5 h and the resulting screen can be used indefinitely if proper maintenance is conducted. Following screen implementation, the screen is cleaned with acetone resulting in no degradation of the photoresist film over the multiple cleaning cycles commenced during this investigation. As a standard office laser printer is used for this process, the minimum attainable resolution that can be achieved in the photoresist film is approximately $225.8 \pm 37.0 \mu\text{m}$ as

Fig. 2 Geometry of a high surface tension fluid progressing across a hydrophilic path in a surface-directed microfluidic device. **a** Isometric view, and **b** side view

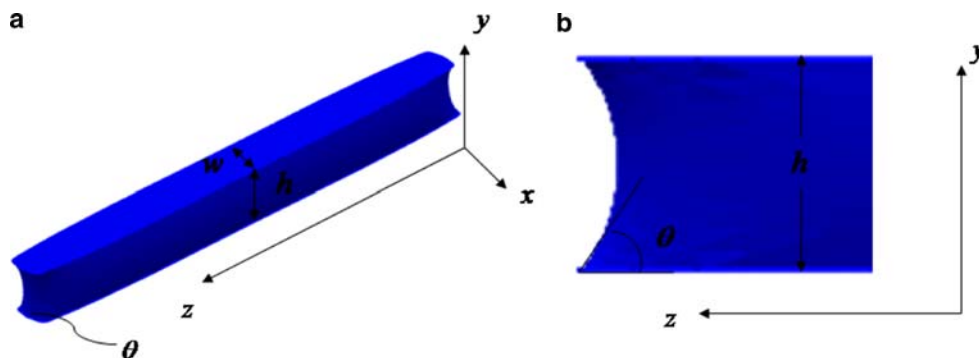


Table 1 Summary of thick film-printed patterns as a function of ink concentration and path width

| Nominal width (μm) | Photomask width (μm) | Screen width (μm) | 8% Width (μm) | 12% Width (μm) | 15% Width (μm) | 18% Width (μm) |
|---------------------------------|-----------------------------------|--------------------------------|----------------------------|-----------------------------|-----------------------------|-----------------------------|
| 300 | 313.2 ± 8.4 | 225.8 ± 37.0 | 242.1 ± 43.6 | 329.2 ± 14.8 | 321.7 ± 12.6 | 313.3 ± 17.9 |
| 550 | 522.1 ± 8.2 | 458.4 ± 37.4 | 381.5 ± 60.7 | 696.8 ± 38.7 | 546.3 ± 14.8 | 583.8 ± 26.1 |
| 800 | 804.2 ± 10.6 | 727.16 ± 23.7 | 419.5 ± 50.5 | 851.3 ± 18.9 | 799.4 ± 26.2 | 830.9 ± 35.5 |
| 1050 | 1068.7 ± 12.1 | 998.2 ± 62.0 | 1036.788.3 | 1122.9 ± 45.2 | 1031.9 ± 17.0 | 1146.9 ± 9.3 |
| 1300 | 1326.6 ± 8.3 | 1293.7 ± 29.4 | 1247.4 ± 43.3 | 1326.3 ± 41.6 | 1318.6 ± 22.1 | 1352.1 ± 16.0 |

determined through optical microscopy of the photoresist film.

2.3 Substrate patterning

Rinzl vinyl microscope slides (Fisher Scientific) reported as PVC by the manufacturer¹ are cleaned with ethanol prior to patterning. Great care must be taken to keep cleaned vinyl slides away from surface contamination as minute amounts of contaminants can drastically affect wettability due to the surface area to volume ratios experienced in microfluidic platforms (Squires and Quake 2005). Thick film ink is prepared from cellulose acetate (39.7% acetylated, $M_n \sim 30,000$, Sigma Aldrich) dissolved in tetraethylene glycol dimethyl ether (Sigma Aldrich), chosen for an inherently low volatility, at various concentrations.

The custom screen is employed for patterning in a MPM TF-100 thick film printer at the Case Electronics Design Center. A small amount of ink is placed directly on the screen in front of the open pattern. The thick film printer squeegee mechanism is actuated and the cellulose acetate ink is pressed through the open pattern in the screen onto the vinyl microscope slide. It is critical that the solvent have sufficiently low volatility as not to evaporate when the ink is in the screen causing the mesh to become blocked by dry polymer. Patterned substrates are placed in vacuum conditions at ambient temperature to cure overnight. After the solvent completely evaporates, the patterned substrates are once again cleaned with ethanol and dried in ambient conditions prior to assembly and implementation. Following the cleansing procedure, preferential wetting is immediately apparent. The adhesion of the cellulose acetate to the PVC slides is rather good. Furthermore, as the PVC and patterned cellulose acetate materials are flexible,

¹ Although this material is reported as PVC by the manufacturer, elemental analysis indicates that 4.19% (w/w) of the material is an element other than hydrogen, chlorine or carbon suggesting that the material is not pure PVC. Furthermore, the presence of a carbonyl band at $1,728 \text{ cm}^{-1}$ demonstrated through Fourier-transform infrared spectroscopy and the flexibility of the material suggests to us that the material is likely a vinyl chloride-vinyl acetate copolymer.

bending of a patterned substrate does not delaminate the hydrophilic film.

A comprehensive investigation on printing resolution was conducted for inks of varying polymer concentration (8, 12, 15 and 18%, w/w). Assorted path widths were printed from nominal CAD values ranging from 300 to 1,300 μm as summarized in Table 1. A total of ten patterns were printed per concentration along with five measurements taken randomly along a path for the determination of path width. As indicated in Table 1 and graphically by Fig. 3, the 8% ink resulted in paths generally below the nominal CAD value as a consequence of the de-wetting of the low viscosity ink. In contrast, the 12% ink tended to be thick enough to flow slightly upon printing but was not capable of de-wetting and forming beaded droplets as in the case of the 8% ink. Both the 15 and 18% inks were found to be relatively close to the CAD design. Figure 3 graphically summarizes the results for this study (Fig. 3).

2.4 Platform assembly

Holes are drilled for fluid introduction at strategically placed locations on the patterned substrates. Opposing patterned substrates are visually aligned and brought within close proximity utilizing $116.4 \pm 7.6 \mu\text{m}$ thick 9,576 double-sided polypropylene film tape (3 M) as determined utilizing a series of micrometer measurements on several assembled devices. The devices of $229.0 \pm 13.9 \mu\text{m}$ were assembled by using a double layer of polypropylene tape. Following alignment, devices are ready for the introduction of an aqueous fluid resulting in autonomous capillary pumping and excellent confinement within intricate geometry in spite of the lack of physical barriers. Care must be taken to keep microfluidic platforms away from airborne contaminants. We have found that storage in ambience results in loss of reproducible function within 1 week. In contrast, storage in a sealed environment seems to inhibit surface contamination leading to the preservation of adequate functionality. However, function can be restored to contaminated devices at any time by simply conducting an additional ethanol cleaning procedure.

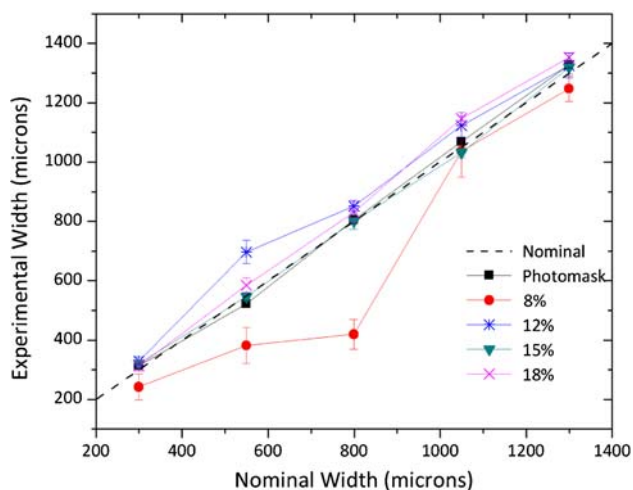


Fig. 3 Graphical summary of thick-film printed paths versus polymer concentration

2.5 Contact angle analysis

The advancing contact angles of the materials were attained utilizing a Ramé–Hart goniometer. A series of five measurements were attained to calculate an average contact angle. The PVC material exhibited a contact angle of $82.4^\circ \pm 1.5^\circ$ while the cellulose acetate contact angle was measured as $60.0^\circ \pm 0.3^\circ$. Both materials have contact angles less than 90° indicating that the fluid is capable of transit across each material via capillarity. However, since there is substantially less resistance for the fluid to progress in the direction of the hydrophilic cellulose acetate, directed flow can be achieved in the microfluidic platform.

2.6 Attaining position–time data

Transparent rulers are fixed to the operational region of the microfluidic platforms. Distilled water is introduced to the platforms and capillary dynamics are recorded on a digital camcorder. The resulting digital media files are converted to mpeg format and analyzed frame by frame with the VirtualDub software package. The resulting data is utilized to construct position versus time curves.

3 Results and discussion

3.1 Demonstration of function

Following the fabrication protocols previously outlined results in microfluidic platforms capable of supporting autonomous fluid transport. From a materials perspective, the resulting devices cost on the order of a penny to manufacture. Furthermore, since screen processing is

relatively simple, a great deal of versatility is attained through the thick film printing process. Figure 4 demonstrates several patterns that have been successfully developed through the thick film printing process along with a variety of solutions utilized within the platforms.

As demonstrated by Fig. 4, the amount of fluid required to implement the surface-tension confined device is in all cases below $20 \mu\text{l}$ of fluid. Furthermore, when implementing the device of minimum resolution ($313.3 \pm 17.9 \mu$ path width, $229.0 \pm 13.9 \mu\text{m}$ gap height), the amount of fluid required is reduced to approximately $2 \mu\text{l}$ in order to transport fluid across a 6.0 cm virtual channel. In addition to dyed-distilled water, the microfluidic platform were also implemented with biologically relevant solutions with drastically different surface tension values than pure water such as phosphate buffered saline (PBS), 1% (w/w) aqueous solution of the surfactant sodium dodecyl sulfate (SDS) and Dulbecco's modified eagle medium (DMEM). The DMEM and PBS solutions maintain rather good confinement across the microfluidic channel. In contrast, directed flow can be achieved with 1% SDS; however, fluid does not maintain excellent confinement across the length of the hydrophilic path.

Furthermore, pattern integrity was investigated as a function of ink viscosity. Viscosities on a weight per weight basis were investigated at concentrations of 8, 12, 15 and 18% cellulose acetate in tetraethylene glycol dimethyl ether. The 8% solution results in a path of very poor integrity leaving the bare substrate exposed as the hydrophilic ink began to de-wet and “bead” on the hydrophobic substrate material. Remarkably, the devices patterned with 8% hydrophilic ink were still capable of supporting autonomous fluid transport although reproducibility is an issue. As ink viscosity increases, pattern integrity becomes substantially better as “beading” becomes inhibited through viscous forces. The 18% solution seems to be the practical limit where cellulose acetate will no longer dissolve into the solvent without extensive heating and agitation. Furthermore, the film thickness of the printed paths were determined through imaging cellulose acetate that was encouraged to delaminate from the PVC substrate with a razor blade. Figure 5 illustrates a typical image attained via scanning electron microscopy demonstrating that film thickness is on the order of approximately one micron. Higher magnification images were unattainable as a consequence of the low melting point of cellulose acetate and heat generated through further focusing of the electron beam.

3.2 Theoretical aspects and characterization

Although a consistent and versatile fabrication procedure exists for the development of surface-directed microfluidic

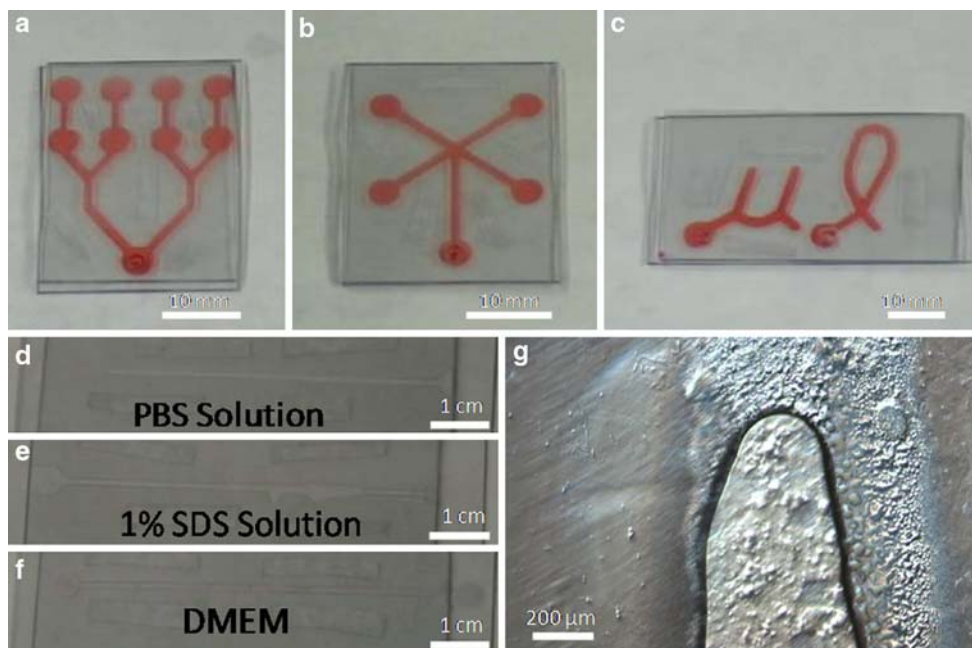


Fig. 4 Demonstration of autonomous surfaced-directed microfluidic platforms. **a** Diverging pattern, 19 μl , **b** Four-well design, 15 μl , **c** Microliter, 15 μl , **d** Device implemented with PBS, **e** SDS, **f** DMEM, and **g** Device with minimum attainable resolution

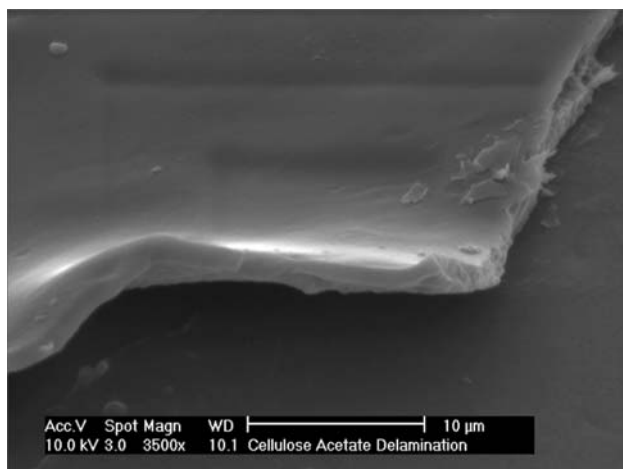


Fig. 5 Scanning electron micrograph indicating relative thickness of a thick film-printed cellulose acetate path encouraged to lift from the substrate material with the tip of a razor blade

devices, a theoretical model is very beneficial for a priori device optimization and intelligent device design with respect to flowrate and residence in support of on-chip reaction processes. The system is defined as a having a symmetrically centered axis with $-w/2 \leq x \leq w/2$ and $-h/2 \leq y \leq h/2$. For the position $x = 0$, end effects are neglected since $h \ll w$. Consequently, the fluid transport is idealized to the canonical flow of an incompressible fluid between parallel plates of infinite width subject to a pressure gradient, dP/dx . Accordingly, an analytical solution exists where μ is the fluid viscosity

$$u(y) = \frac{1}{2\mu} \left[y^2 - \frac{h^2}{4} \right] \frac{dP}{dx}. \quad (3)$$

Although relation (3) incorrectly describes the concavity of the profile of the advancing front, the relationship between velocity versus a pressure gradient correctly represents the physics of surface-directed microfluidic platform. Moreover, since the curvature of the front is indiscernible from a macroscopic perspective, one can assume the centerline velocity is an adequate approximation for the overall fluid filament velocity

$$u(0) \approx u = \frac{-h^2 dP}{8\mu dx}. \quad (4)$$

Neglecting edge effects, it is possible to utilize the Laplace pressure as an approximate pressure drop dependent upon the fluid surface tension γ and the advancing contact angle θ assuming contact angle dynamics are negligible

$$\frac{dP}{dx} \approx \frac{\Delta P}{x} = \frac{-2\gamma \cos \theta}{h}. \quad (5)$$

Incorporating relation (5) into relation (4), an analytical expression for the velocity is established

$$u = \frac{h\gamma \cos \theta}{4\mu x}. \quad (6)$$

Integrating relationship (6) with respect to x from 0 to L with respect to time from 0 to t applying the initial condition of a distance of $x = 0$ at $t = 0$ results in an analytical relationship for position as a function of time

$$L(t) = \left[\frac{h\gamma \cos \theta}{2\mu} t \right]^{1/2} \tag{7}$$

This result agrees with the model posed by Yang et al. (2004), and demonstrates the $t^{1/2}$ dependency on position demonstrated for capillary-driven microfluidic platforms of alternative geometry (Mann Jr. et al. 1995; Romero and Yost 1996; Rye et al. 1996a, b; Zhmud et al. 2000) or fabrication approach (Bouaidat et al. 2005).

From result (7), one finds that a characteristic diffusion constant, D , exists for this system dependent upon system architecture, fluid properties and fluid–substrate energetic interactions

$$D = \frac{h\gamma \cos \theta}{2\mu} \tag{8}$$

For pure water at 20°C in contact with the PVC material, D is $5.6 \times 10^{-4} \text{ m}^2/\text{s}$ and $1.1 \times 10^{-3} \text{ m}^2/\text{s}$ for gap heights of 116.4 and 229.0 μm , respectively.

Results were attained utilizing ten independent devices patterned with 18% (w/w) ink solutions with the three largest path widths (i.e., large widths chosen to eliminate inconsistencies associated with misalignment of the visually assembled devices). The results indicate good agreement with the theoretical model (Fig. 6). Figure 6a, b demonstrate the relationship of distance as a function of time. The theoretical model was also implemented

with one standard deviation in the contact angle of the PVC material. The experimental data was also linearized for Fig. 6c, d in order to exhibit the deviation in time measurements as the fluid progressed a specified distance.

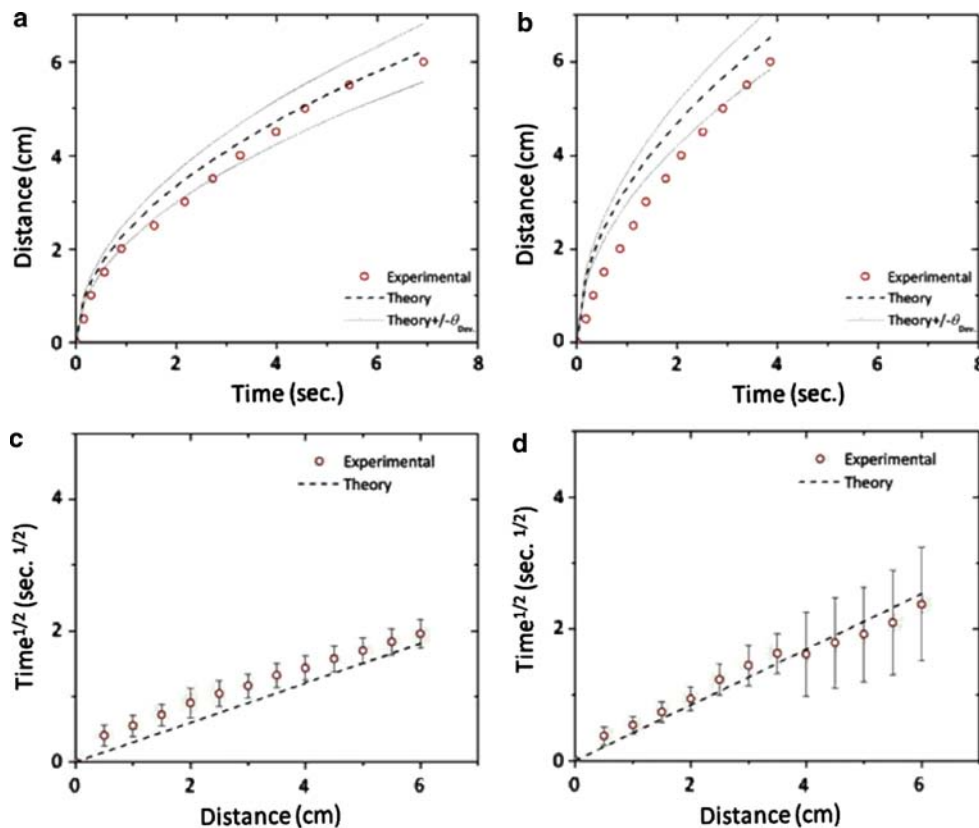
As predicted by expression (7), the meniscus position is not directly dependent upon the path width. Moreover, the system dynamics are dependent upon the hydrophobic contact angle rather than the hydrophilic contact angle. This result seems fortuitous at first. However, this is an implication of choosing a hydrophobic material with a contact angle less than 90°. Specifically, the outside layer of the fluid is able to slightly bleed into the hydrophobic region. Consequently, the progression of the meniscus is rate limited by the maximum velocity that can be achieved for a fluid progressing across the hydrophobic PVC substrate material.

Furthermore, considering the a characteristic length of a hydraulic diameter (i.e., four times the cross-sectional area divided by the perimeter) and differentiating relation (7) with respect to time allows for the development of a relation for the dynamic Reynolds number

$$\text{Re} = \frac{\rho}{\mu} \frac{wh}{(w+h)} \frac{D}{\sqrt{Dt}} \tag{9}$$

The resulting proportionality of velocity to the inverse of the square-root of time is consistent with results previously

Fig. 6 Capillary dynamics as a function of time and system architecture for (a), (c) heights of 116.4 μm , and (b), (d) 229.0 μm



published (Chen et al. 2006). Expression (9) can be solved to find the amount of time required for the Reynolds number to drop into the laminar regime ($Re \leq 2,000$). For the system capable of the most rapid flow, with a gap height of $229.0 \mu\text{m}$ and width of $1352.1 \mu\text{m}$, the time requirement to achieve laminar flow in the surface-directed device is $10.5 \mu\text{s}$ indicating fully developed flow is achieved quickly. This suggests that the assumption of negligible contact angle dynamics is plausible. Furthermore, this result indicates that capillary flow alone does not result in mixing within the device.

Furthermore, employing the Monge representation, it is possible to calculate the curvature associated pressure jump, $[p]$, across the advancing interface enabling the

quantification of the capillary driving force at every point upon the advancing free surface. Specifically, using the general Laplace equation, the pressure jump is related to the fluid surface tension and mean curvature H , viz

$$[p] = 2\gamma H. \quad (10)$$

Consequently, calculating the curvature of the interface directly enables the determination of the pressure jump at any point upon the fluid–gas interface as opposed to utilizing a spatially constant Laplace pressure approximation. However, before this can be done, the Monge representation must be implemented mapping a 2D surface to a 3D surface (Mann 2002)

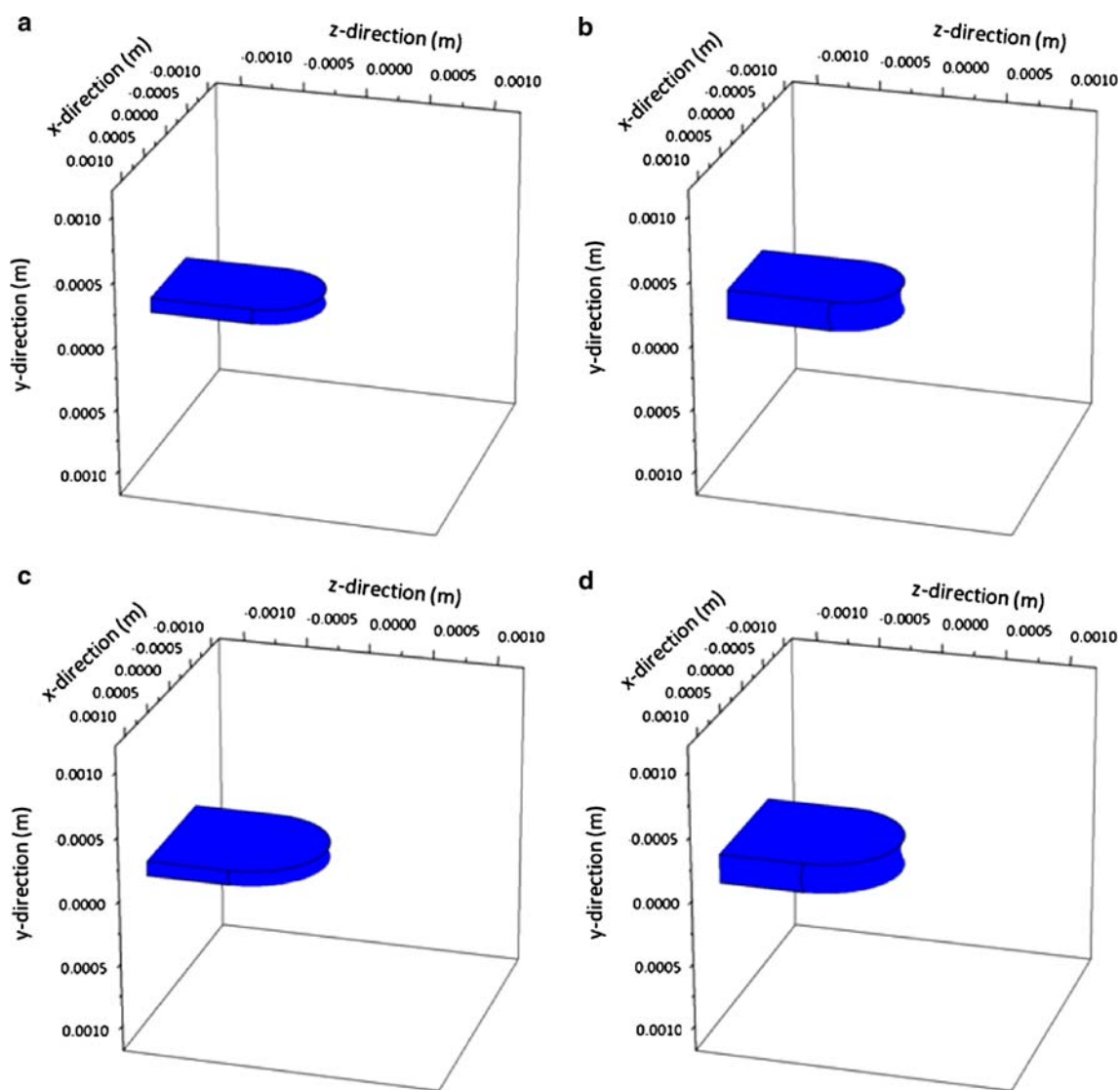


Fig. 7 Reconstructed surfaces utilizing the Monge surface representation. **a** $w = 830.9 \mu\text{m}$, $h = 116.4 \mu\text{m}$, **b** $w = 830.9 \mu\text{m}$, $h = 229.0 \mu\text{m}$, **c** $w = 1146.9 \mu\text{m}$, $h = 116.4 \mu\text{m}$, and **d** $w = 1146.9 \mu\text{m}$, $h = 229.0 \mu\text{m}$

$$\Sigma_t := \begin{cases} x = u^1 \\ y = u^2 \\ z = \zeta(u^1, u^2, t) \end{cases} \quad (11)$$

The two dimensional surface is a rectangular patch of dimensions $-w/2 \leq u^1 \leq w/2$ and $-h/2 \leq u^2 \leq h/2$ which is mapped to a three dimensional curved surface of the advancing fluid meniscus. Assuming the surface is sufficiently smooth, as mandated by physical energetics, and that the surface can be approximated adequately by using the minimum and maximum radii of curvature, it is possible to fit the advancing surface to two functions each contributing to the surface curvature independent of the other [$L(t)$ is the dynamic contribution directly from expression (7)]

$$\zeta_1(u^1) = -\frac{w}{2} + \left[\frac{w^2}{4} - (u^1)^2 \right]^{1/2} \quad (12)$$

$$\zeta_2(u^2) = \frac{h}{2 \cos \theta} + \left[\frac{h^2}{4(\cos \theta)^2} - (u^2)^2 \right]^{1/2} \quad (13)$$

$$\zeta(u^1, u^2, t) = L(t) + \zeta_1(u^1) + \zeta_2(u^2). \quad (14)$$

For $\zeta_2(u^2)$ the contact angle considered is the hydrophilic material contact angle across the width of the path, w . In this approach, the Monge model implicitly assumes the hydrophobic region has a contact angle of $\pi/2$. Therefore,

utilizing this idealization, the pressure jump does not depend on contact angle competition.

Consequently, the advancing front can be reconstructed for any given time via mapping $R^2 \rightarrow R^3$. Furthermore, the mean curvature of the surface can be explicitly calculated where the subscripts denote the spatial derivative taken for each associated term

$$H = \frac{(1 + \zeta_{u^1}^2)\zeta_{u^2 u^2} - 2\zeta_{u^1} \zeta_{u^2} \zeta_{u^1 u^2} + (1 + \zeta_{u^2}^2)\zeta_{u^1} \zeta_{u^1}}{2(1 + \zeta_{u^1}^2 + \zeta_{u^2}^2)^{3/2}} \quad (15)$$

Considering a fluid meniscus advancing upon the hydrophilic cellulose acetate material, the curvature based pressure jump has been explicitly calculated. Figure 7 demonstrates the structure of the advancing fluid front for the four architectures investigated in this study. Figure 8 and Table 2 summarize the calculated results for interfacial pressure jump versus the approximated result.

The approximated pressure jump is computed directly from the Laplace pressure approximation where θ_P is the contact angle of the polar hydrophilic material and θ_N is the contact angle of the non-polar hydrophobic material (Delamarche et al. 1998; Juncker et al. 2002)

$$\Delta P = 2\gamma \left[\frac{\cos \theta_P}{h} + \frac{\cos \theta_N}{w} \right] \quad (16)$$

The averaged pressure jump is a length-normalized Frobenius norm of the discretized $n \times n$ pressure jump matrix

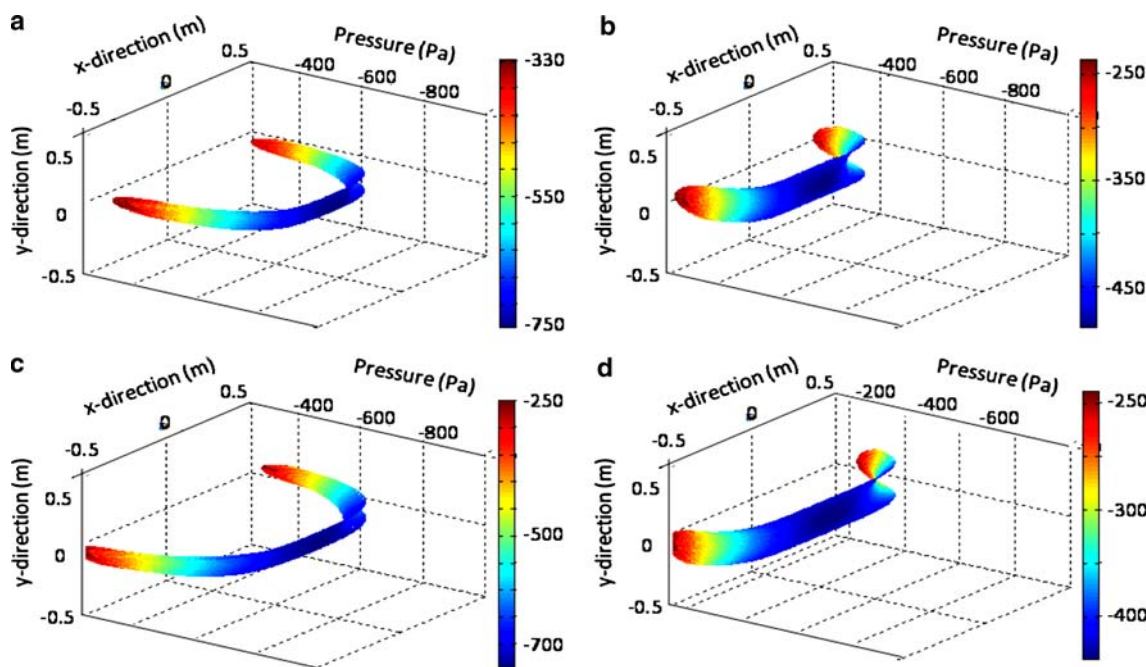


Fig. 8 Predicted pressure jump across gas–liquid interface for all configurations investigated. **a** $w = 830.9 \mu\text{m}$, $h = 116.4 \mu\text{m}$, **b** $w = 830.9 \mu\text{m}$, $h = 229.0 \mu\text{m}$, **c** $w = 1146.9 \mu\text{m}$, $h = 116.4 \mu\text{m}$, and **d** $w = 1146.9 \mu\text{m}$, $h = 229.0 \mu\text{m}$

Table 2 Summary of calculations and comparison to the Laplace pressure approximation

| Gap height (μm) | Path width (μm) | Laplace approximation pressure jump (Pa) | Averaged curvature pressure jump (Pa) | Minimum pressure jump (Pa) | Maximum pressure jump |
|------------------------------|------------------------------|--|---------------------------------------|----------------------------|-----------------------|
| 116.4 | 830.9 | -641.5 | -683.8 | -791.8 | -297.0 |
| 116.4 | 1146.4 | -337.3 | -430.5 | -487.7 | -236.2 |
| 229.0 | 830.9 | -635.2 | -637.6 | -744.0 | -249.3 |
| 229.0 | 1146.4 | -331.0 | -383.9 | -439.9 | -188.4 |

$$[p]_{\text{Avg.}} = \frac{1}{n} \left[\sum_{j=1}^n \sum_{i=1}^n [p]_{ij}^2 \right]^{1/2} \quad (17)$$

As demonstrated by Table 1, the curvature-based calculations are in good agreement. Moreover, as the height decreases, the curvature-based calculation begins to converge upon the Laplace result. This result arises from the fact that as height decreases, the hydrophilic contact angle term begins to dominate in the pressure jump calculation.

The higher-dimensional mapping technique produces a smooth surface which can be exploited for the quantitative characterization of the driving force for the microfluidic system. The method yields a position-dependent pressure jump as opposed to the constant Laplace pressure approximation. Consequently, the Monge surface mapping technique is a more accurate depiction of the true physics involved with surface-directed microfluidic capillary transport.

4 Concluding remarks

As novel methods are established for the manipulation of micro-volumes of fluids, the amount of invasive or expensive reagents required for chemical or biological analyses is decreased while throughput and parallelization is increased. The automation of such analyses will enable a user with little to no analytical experience to conduct sophisticated laboratory procedures. However, before such technology can be exploited, microfluidic chip processing techniques need to be re-evaluated and optimized in order to make this technology affordable for wide-scale deployment.

The thick film printing technique is a straight-forward fabrication approach toward developing autonomous microfluidic platforms. As thick film printing is a well-characterized patterning technology, patterning is rather uncomplicated and ultimately scalable into a continuous mass-production scheme. Furthermore, as commodity polymeric materials are utilized, the total cost of platform production is minimal. Subsequently, the thick-film printed microfluidic fabrication approach solves a number of manufacturing dilemmas inhibiting wide-scale deployment of microfluidic “lab on a chip” technologies.

In addition to explicating the fabrication approach, theoretical framework has been established enabling intelligent platform design for the integration of chip-based reaction processes. As a result, surface-directed microfluidics is ready to be implemented for novel applications. Such applications are currently under investigation by the authors of this article.

Acknowledgments We gratefully acknowledge the Infoscitex Corp. (Waltham, MA, USA) and the Air Force Research Laboratory, Human Effectiveness Directorate, Applied Biotechnology Branch for partial financial support of this work. Furthermore, we thank Laurie Dudik and the Case Electronics Design Center and Michael Cushman of IST in particular for many fruitful discussions regarding the device design and manufacturing.

References

- Adamson AW, Gast AP (1997) Physical chemistry of surfaces, 6th edn. Wiley-Interscience, New York
- Bouaidat S, Hansen O, Bruus H, Berendsen C, Bau-Madsen NK, Thomsen P, Wolff A, Jonsmann J (2005) Surface-directed capillary system; theory, experiments and applications. *Lab Chip* 5:827–836
- Brakke KA (1992) The surface evolver. *Exp Math* 1:141–165
- Burns MA (1998) An integrated nanoliter DNA analysis device. *Science* 282:484–487
- Butler JE, Lue EP, Navarro P, Christiansen B (1997a) Comparative studies on the interaction of proteins with a polydimethylsiloxane elastomer. I. Monolayer protein capture capacity (PCC) as a function of protein pl, buffer pH and buffer ionic strength. *J Mol Recognit* 10:36–51
- Butler JE, Navarro P, Lue P (1997b) Comparative studies on the interaction of proteins with a polydimethylsiloxane elastomer. II. The comparative antigenicity of primary and secondarily adsorbed IgG 1 and IgG 2 a and their non-adsorbed counterparts. *J Mol Recognit* 10:52–62
- Chen CF, Kung CF, Chen HC, Chu CC, Chang CC, Tseng FG (2006) A microfluidic nanoliter mixer with optimized grooved structures driven by capillary pumping. *J Micromech Microeng* 16:1358–1365
- Choban ER, Markoski LJ, Wieckowski A, Kenis PJ (2004) Microfluidic fuel cell based on laminar flow. *J Power Sources* 128:54–60
- Delamarche E, Bernard A, Schmid H, Bietsch A, Michel B, Biebuyck H (1998) Microfluidic networks for chemical patterning of substrates: design and application to bioassays. *J Am Chem Soc* 120:500–508
- Etshola E, Balberg M (2004) Microfluidic ELISA: on-chip fluorescence imaging. *Biomed Microdevices* 6:7–9

- Eteshola E, Leckband D (2001) Development and characterization of an ELISA assay in PDMS microfluidic channels. *Sens Actuators B* 72:129–133
- Goodwin SB, Schneider RE, Fry WE (1995) Use of cellulose-acetate electrophoresis for rapid identification of allozyme genotypes of *Phytophthora infestans*. *Plant Dis* 79:1181–1185
- Holmes EPJ (1976) *Handbook of thick film technology*. 2 edn. Emerald Group Publishing Limited, Bradford
- Jayashree RS, Gancs L, Choban ER, Primak A, Natarajan D, Markoski LJ, Kenis PJA (2005) Air-breathing laminar flow-based microfluidic fuel cell. *J Am Chem Soc* 127:16758–16759
- Juncker D, Schmid H, Drechsler U, Wolf H, Wolf M, Michel B, de Rooij N, Delamarche E (2002) Autonomous microfluidic capillary system. *Anal Chem* 74:6139–6144
- Khandurina J, McKnight TE, Jacobson SC, Waters LC, Foote RS, Ramsey JM (2000) Integrated system for rapid PCR-based DNA analysis in microfluidic devices. *Anal Chem* 72:2995–3000
- Lagally ET, Simpson PC, Mathies RA (2000) Monolithic integrated microfluidic DNA amplification and capillary electrophoresis analysis system. *Sens Actuators B* 63:138–146
- Lam P, Wynne KJ, Wnek GE (2002) Surface-tension-confined microfluidics. *Langmuir* 18:948–951
- Mann JA (2002) A free energy model for curved surfaces and curved thin films in emulsions. *J Dispersion Sci Tech* 23:199–207
- Mann Jr JA, Romero L, Rye RR, Yost FG (1995) Flow of simple liquids down narrow V-grooves. *Phys Rev E* 52:3967–3972
- Marengo-Rowe AJ (1965) Rapid electrophoresis and quantitation of haemoglobin on cellulose acetate. *J Clin Pathol* 18:790–792
- Mastrangelo CH, Burns MA, Burke DT (1998) Microfabricated devices for genetic diagnostics. *Proc IEEE* 86:1769–1787
- Meera Khan P (1971) Enzyme electrophoresis on cellulose acetate gel: zymogram patterns in mgh-mouse and man—Chinese hamster somatic cell hybrids. *Arch Biochem Biophys* 145:470–483
- Mitrovski SM, Elliott LCC, Nuzzo RG (2004) Microfluidic devices for energy conversion: planar integration and performance of a passive, fully immersed H₂-O₂ fuel cell. *Langmuir* 20:6974–6976
- Nag A, Panda BR, Chattopadhyay A (2005) Performing chemical reactions in virtual capillary of surface tension-confined microfluidic devices. *Pramana J Phys* 65:621–630
- Oh CS (1999) Microfluidic electrophoresis device. United States Patent 5,904,824
- Romero LA, Yost FG (1996) Flow in an open channel capillary. *J Fluid Mech* 322:109–129
- Rye RR, Mann JJA, Yost FG (1996a) The flow of liquids in surface grooves. *Langmuir* 12:555–565
- Rye RR, Yost FG, Mann JA Jr (1996b) Wetting kinetics in surface capillary grooves. *Langmuir* 12:4625–4627
- Sato K, Yamanaka M, Hagino T, Tokeshi M, Kimura H, Kitamori T (2004) Microchip-based enzyme-linked immunosorbent assay (microELISA) system with thermal lens detection. *Lab Chip* 4:570–575
- Squires TM, Quake SR (2005) Microfluidics: fluid physics at the nanoliter scale. *Rev Mod Phys* 77:977–1026
- Suk JW, Cho JH (2007) Capillary flow control using hydrophobic patterns. *J Micromech Microeng* 17:N11–N15
- Watanabe M (2007) Refreshable microfluidic channels constructed using an inkjet printer. *Sens Actuators B Chem* 122:141–147
- West J, Michels A, Kittel S, Jacob P, Franzke J (2007) Microplasma writing for surface-directed millifluidics. *Lab Chip* 7:981–983
- White NM, Turner JD (1997) Thick-film sensors: past, present and future. *Meas Sci Technol* 8
- Yang LJ, Yao TJ, Tai YC (2004) The marching velocity of the capillary meniscus in a microchannel. *J Micromech Microeng* 14:220–225
- Zhao B, Moore JS, Beebe DJ (2001) Surface-directed liquid flow inside microchannels. *Science* 291:1023–1026
- Zhao B, Moore JS, Beebe DJ (2002) Principles of surface-directed liquid flow in microfluidic channels. *Anal Chem* 74:4259–4268
- Zhmd BV, Tiberg F, Hallstenson K (2000) Dynamics of capillary rise. *J Colloid Interface Sci* 228:263–269